stellarator news

Published by Fusion Energy Division, Oak Ridge National Laboratory
Building 9201-2 P.O. Box 2009 Oak Ridge, TN 37831-8071, USA

Editor: James A. Rome Issue 85 January 2003
E-Mail: jar@ornl.gov Phone (865) 574-1306
On the Web at *http://www.ornl.gov/fed/stelnews*

NCSX and QPS receive favorable program reviews

The proposed U.S. compact stellarators NCSX (National Compact Stellarator Experiment) and QPS (Quasi-poloidal Stellarator) were reviewed by their advisory committees during December. 2002

NCSX

The NCSX Program Advisory Committee (PAC) held its sixth meeting on December 9–10 at the Princeton Plasma Physics Laboratory (PPPL). The committee advises PPPL on planning and priorities for NCSX and its other stellarator research activities and has been meeting since 1998.

At the PAC-6 meeting, the committee was asked to review the progress on NCSX since the May 2002 conceptual design review (CDR) and to advise on the project's preparations for the next review, a preliminary design review (PDR) planned for June 2003. Members of the NCSX team described design improvements that have been made to increase physics flexibility, reduce engineering risks, and streamline the fabrication process. They also described the plans for design development, analysis, and testing activities to the support the PDR. Optimizing the vacuum vessel port arrangement to meet diagnostic needs was highlighted as a key integration task for this period.

In a preliminary summary of the meeting's conclusions, PAC chair Professor David Anderson (Univ. of Wisconsin) commended the progress that has been made in the design of the NCSX modular coils and vacuum vessel. He said that changes in the coil design since the CDR were responsive to earlier PAC recommendations to emphasize divertor issues and that the PAC agreed with the project's plan to freeze the coil design at this time. Anderson listed several committee recommendations to improve the planning in the areas of physics analysis, diagnostic priorities, and engineering design and R&D. In addition, the PAC provided many valuable suggestions to guide the planning of PPPL's stellarator research program for the next several years. Members attending the PAC-6 meeting were D. Anderson (Univ. of Wisconsin), Chair, B. Blackwell (Australian National Univ.), M. Greenwald (Massachusetts Institute of Technology), C. Hegna (Univ. of Wisconsin), D. Hill (Lawrence Livermore National Laboratory), S. Knowlton (Auburn Univ.), T. Luce (General Atomics), S. Luckhardt (Univ. of California at San Diego), J. Menard (Princeton Plasma Physics Laboratory), D. Newman (Univ. of Alaska at Fairbanks), S. Okamura (National Institute for Fusion Science, Japan), D. Ross (Univ. of

In this issue . . .

Texas at Austin), A. Weller (Max Planck Institute for Plasma Physics, Germany), and H. Weitzner (New York Univ.).

G. H. Neilson
Princeton Plasma Physics Laboratory
Princeton, NJ 08544
E-mail: hneilson@pppl.gov

QPS

The QPS Project Advisory Committee (PAC) met on 11–12 December to analyze the QPS Team's preparations for the April 2003 CDR by the Department of Energy. The QPS PAC is drawn from experts in stellarator physics, compact stellarator design, and toroidal confinement physics: H. Weitzner (New York Univ., chair), D. Anderson (Univ. of Wisconsin), B. Blackwell (Australian National Univ.), S. Kaye (PPPL), S. Knowlton (Auburn Univ.), H. Kugel (PPPL), S. Luckhardt (Univ. of California at San Diego), G. H. Neilson (PPPL), S. Okamura (National Institute for Fusion Science, Japan), W. Reiersen (PPPL), A. Weller (Max Planck Institute for Plasma Physics, Germany), and M. Zarnstorff (PPPL). The PAC was asked to advise Oak Ridge National Laboratory on all aspects of the QPS team's preparations for the CDR.

Members of the QPS team described (1) the QPS mission, project status, and disposition of issues from the April 2001 Physics Validation Review; (2) the experimental plan; (3) the physics properties and flexibility of QPS; (4) an engineering design overview; (5) power and particle control and vacuum conditioning; and (6) project implementation. The QPS presentations to the PAC can be found on the QPS web site at

http://qps.fed.ornl.gov/

The PAC summarized its findings as follows: "The committee commends the QPS team on their excellent work on the physics and engineering design of the QPS experiment. The physics design is well documented in terms of equilibrium properties, stability, and neoclassical transport. The optimization of the configuration is also clearly shown. The engineering design is very well developed for this phase of the program and the most appropriate R&D efforts and analyses needed for the CDR are underway." In addition, the PAC had a number of suggestions on strengthening the team's preparations for the QPS CDR, primarily in the areas of experimental planning, rf heating scenarios, access to the interior of the vacuum vessel, issues relating to the modular coil cases, field error calculations, and conduct of the program.

J. F. Lyon
Oak Ridge National Laboratory
Oak Ridge, TN 37831-8072
E-mail: lyonjf@ornl.gov

The effect of boronization on turbulent fluctuations in the core and edge plasma of the L-2M stellarator

In a recent experimental campaign (2001–2002) on the L-2M stellarator (General Physics Institute, Moscow), turbulent plasma fluctuations were studied in discharges with preliminary boronization of the vacuum chamber. A plasma was created and heated by microwave gyrotron radiation at the second harmonic of the electron gyrofrequency. The experiments were intended to clarify the following questions:

- Is it possible to reduce the influence of an influx of gas from the walls of the vacuum chamber on a local fluctuating particle flux by boronizing the chamber walls?
- How does boronization affect the characteristics of coherent spatial-temporal structures in the toroidal direction and their radial dependences?
- Can we be assured of a rather high degree of coherence between plasma density fluctuations in the center of the plasma column and at the edge?

We do not go into details of the boronization procedure here. We list only the plasma characteristics measured and the diagnostics employed for these measurements to answer the above questions.

Attention was concentrated on the behavior of the plasma density fluctuations δn and the local fluctuating particle flux $\delta\Gamma$. Density fluctuations were measured both at the plasma edge and in the central region of the plasma column, whereas the fluctuating particle flux was measured only at the edge. Fluctuations in the edge plasma were measured with the help of radial movable Langmuir probes, described in detail in Ref. [1]. Two sets of such probes were installed in different poloidal sections, the distance between them being 2.2 m along the torus. The probe measurements yielded the radial distributions of the plasma density $n(r/r_s)$, the floating potential $U_f\,(r/r_s)$, and the amplitude of plasma density fluctuations $(\delta n/n)(r/r_s)$ (here, r is the mean magnetic-surface radius, and r_s is the mean separatrix radius). Plasma density fluctuations in the central region were measured, as in Ref. [2], from signals of the gyrotron radiation scattered by these fluctuations at angle $\pi/2$. Data were recorded with the help of fast analog-to-digital converters with a sampling rate from 1 to 40 MHz. In data processing, we used the current methods for spectral and statistical-probabilistic analyses.

We now turn to the results of these measurements. Figure 1 shows the radial floating-potential distributions $U_f\,(r/r_s)$

measured before and after boronization of the chamber walls. First, we should mention that the reproducibility of the radial distributions $U_f\ (r/r_s)$ and $(\delta n/n)\ (r/r_s)$ from one shot to the next was better following boronization than it was during the previous operational regimes. The difference goes still further. As can be seen from the figure, before boronization, a change in the sign of U_f occurred in the deeper layers of the plasma. This is evidence that the radial electric field in the edge plasma takes on a different value in the regime with boronization. The change in the sign of U_f in the deeper layers without boronization can be explained as a result of lower electron temperature at the edge because of cooling by the gas coming from the walls. Boronization does not exert a dramatic effect on the character of the distribution $n(r/r_s)$ (the density gradient is somewhat increased), but the amplitude of plasma density fluctuations decreases markedly.

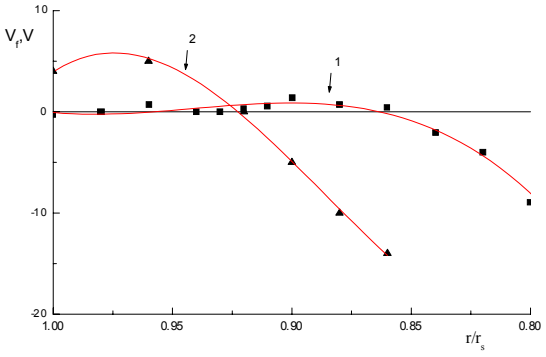

Fig.1. Radial distribution of floating potential: (1) shots 47223–47232 before boronization, and (2) shots 52985–52992 after boronization.

The local fluctuating particle flux $\delta\Gamma$ in the edge plasma and its characteristics demonstrate a favorable effect of boronization. As an example, the fluctuating particle flux $\delta\Gamma$ in real time is shown in Fig. 2. Notice that this flux is directed predominantly outward (this direction corresponds to positive amplitudes in the figure) during the entire discharge. Such behavior is different from that in the regime without boronization, when the direction of $\delta\Gamma$ varied during a discharge and hence also from shot to shot, being sensitive to incidental variations in the inflow of gas from the walls. The constructed probability density function (PDF) for $\delta\Gamma$ allows us to clearly recognize the prevailing direction of the local fluctuating flux. Figure 3 shows the PDF for $\delta\Gamma$ averaged over several shots. The skewness and kurtosis values are also shown. The PDF of $\delta\Gamma$ demonstrates an appreciable deviation from a Gaussian, which is more pronounced for $\delta\Gamma$ with comparatively large amplitudes.

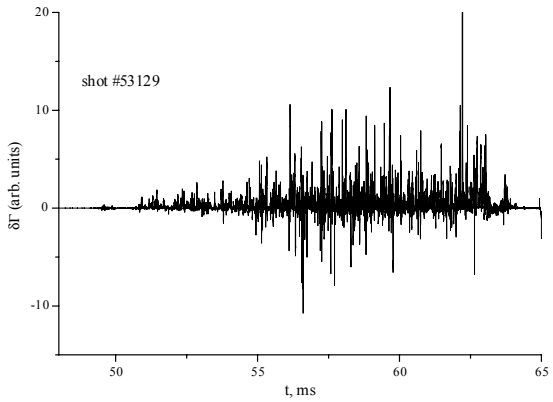

Fig. 2. Local fluctuating particle flux.

The toroidal wavelet coherence for δn and the local fluctuating particle flux $\delta\Gamma$ were also examined for discharges with preliminary boronization. The coefficient of toroidal coherence for these variables turned out to be relatively high, reaching 0.3–0.7 for δn in the frequency range 25–200 kHz (Fig. 4).

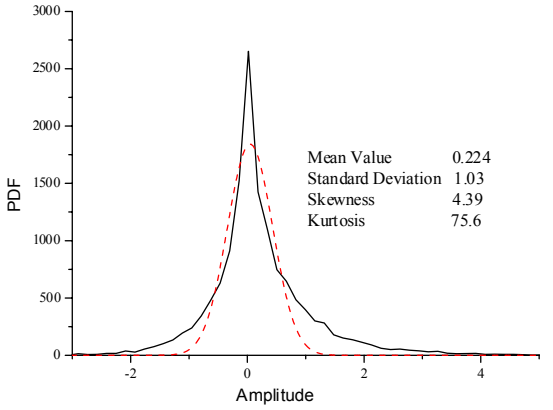

Fig. 3. The probability density function of the local fluctuating particle flux averaged over seven shots (#53266, 68, 69, 71, 78, 79, 80). The best fit to a Gaussian distribution is shown by a red dashed line. The distribution moments are listed on the figure.

For probe sets positioned at different magnetic surfaces (r ~ 1 cm), we also observed a substantial (0.3–0.4) toroidal wavelet coherence between fluctuations δn in the same frequency range. As for the local fluctuating flux $\delta\Gamma$, the toroidal wavelet coherence on the same distance, 2.2 m, was somewhat lower and was estimated at 0.3–0.5 for a narrower frequency range, 25–100 kHz. As mentioned above, the characteristics of the plasma density fluctuations δn in the central region of the plasma column were

measured from the scattered heating gyrotron radiation at a fixed scattering angle $\pi/2$. In this run of experiments, the wavelet coherence between density fluctuations δn in the center and at the edge of the plasma column turned out to be close to the value obtained previously in Ref. [2]; it was estimated to be 0.3–0.5 for a frequency range from 25–30 kHz to 100 kHz.

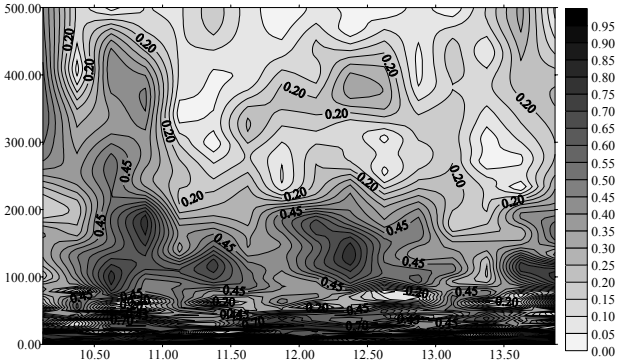

Fig. 4. Toroidal wavelet coherence between the saturation ion currents δI_s ($\delta I_s \sim \delta n$) of two probes located 6–8 mm inside the separatrix; the distance between the probes is 2.2 m along the torus. Shot 53249. The ordinate is the frequency (kHz). The value of the coherence coefficient is shown by the shade of gray.

The results obtained can be summarized as follows:

- Boronization significantly reduced the adverse effect of the influx of gas from the walls, thus providing stable operation and good reproducibility of measurements of fluctuating plasma parameters.
- In the regime with preliminary boronization, the prevailing direction of the local fluctuating particle flux in the edge plasma is outward from the plasma.
- Reliable statistical data on toroidal coherence of plasma density fluctuations could be obtained in this regime. The coefficient of toroidal coherence reached 0.5–0.7 in the frequency range 25–200 kHz, and the coherence region is spanned by at least 1 cm in the radial direction.
- The previous conclusion of the existence of coherence between plasma density fluctuations in the central region and at the edge was confirmed in these experiments with preliminary boronization of the chamber.

Acknowledgment

This work was supported by the Russian Foundation for Basic Research (project N 00-02-01-02-16527).

References

[1] G. M. Batanov, O. I. Fedianin, N. K. Kharchev, et al., Plasma Phys. Controlled Fusion **40** (1998) l241.

[2] G. M. Batanov, L. V. Kolik, A. E. Petrov, et al., JETP Lett. **72** (2000) 174.

K. A. Sarksyan for the L-2M Team
General Physics Institute
Moscow, Russia
E-mail: sarksian@fpl.gpi.ru
Phone: 7-095-135-80-39

A breakthrough to increase neutral beam injection power

In the Large Helical Device (LHD, Toki, Japan), neutral beam injection (NBI) is one of the most powerful and promising methods of heating a plasma to increase the plasma parameters, and also of generating a target plasma [1]. Increasing the injection power can be expected to improve the physics parameters of plasma experiments and also to support the achievement of the target values. These target values are a power of 5 MW/beam line, an energy of 180 keV, and a beam pulse duration of 10 s. In order to increase injection power and to partially achieve the mission, a new design for a negative ion source was investigated. The element with the most radical change is the accelerator. Here we report on the beam characteristics of this new type of negative ion source as installed on an LHD beam line.

Scheme of the new accelerator

The largest change in the new ion source is in the beam accelerator. In LHD the H^- beam energy range is 100–180 keV. A single-stage accelerator has been used for H^- beam formation. A schematic view of the previous beam accelerator is shown in Fig.1. The *z*-axis is defined parallel to the H^- beam. Negative hydrogen ions are produced in a cesium seeded arc chamber, which is to the left of the plasma grid (PG). The H^- beam is extracted from the plasma grid to the extraction grid (EG). Inside the EG, permanent magnets are installed to sweep out the electrons extracted with the H^- beam. The negative ion beam is then formed by applying an acceleration voltage between the EG and a multi-aperture grounded grid (MAGG). The bottom of Fig. 1 shows one of five sections of the grounded grid which are aligned in the *y*-direction. Each row of apertures is shifted alternately in order to correct the trajectories of individual H^- beamlets deflected by the magnets installed in the EG.

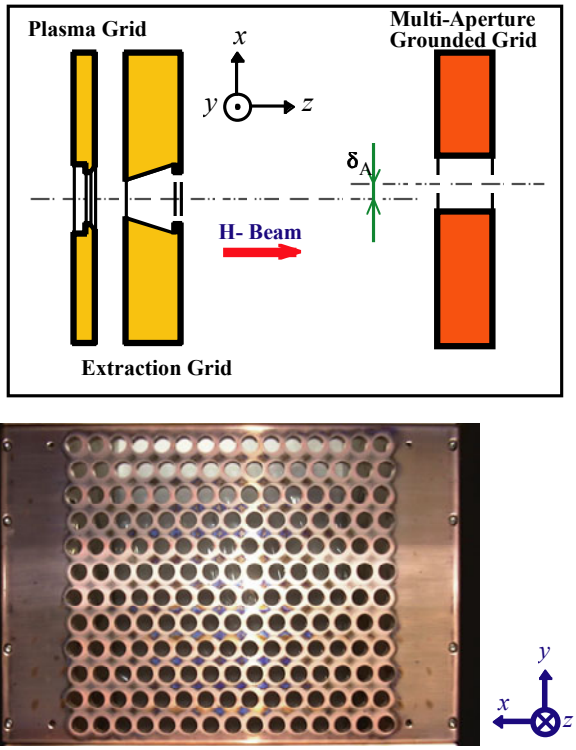

Fig. 1. The MAGG-based beam acceleration system, previously used to produce negative ion beams for NBI on LHD. Top: Schematic view of the beam accelerator. Here the H^- beam direction is defined parallel to *z*-axis. The aperture displacement δ_A corrects the trajectories of the individual H^- beamlets. Bottom: A sample MAGG. The alternating shift in the rows of apertures in the *x*-direction correct the trajectories of individual H^- beams.

The new type grounded grid has no circular aperture. The grid consists of racetrack-like slits elongated in the *x*-direction and we call the grid a multi-slit grounded grid (MSGG). A schematic view of the new accelerator with MSGG is shown in Fig. 2(Top) and a photograph of the grid is shown in Fig. 2(Bottom). The MSGG is not able to correct the H^- beam trajectories in the *x*-direction, so a steering grid is added near the extraction grid.

The main sources of heat loads onto the grounded grid are leakage electrons through EG, out of focus H^- ions, and H^o beams neutralized by collisions of the H^- beam with neutral gas inside the acceleration gap, stripping its electrons. These species are inevitable and to reduce heat load a reduction of the surface area of the grounded grid is required. By changing ground grid from MAGG to MSGG the transparency increases from 35.4% to 61.5%. Furthermore, the stripping loss [2], which causes the H^o beam and the stripped electrons, is a simple increasing function of a gas pressure, and the gas load inside acceleration gap can be decreased by increasing the transparency of grounded

grid Therefore the MSGG acceleration system is expected to have a reduced heat load onto the grid.

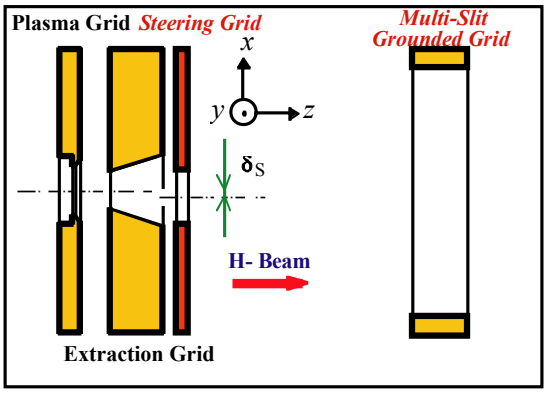

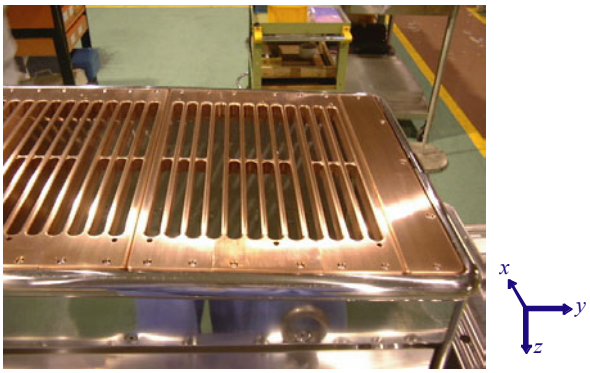

Fig. 2. The MSGG-based beam acceleration system in the new negative ion source for NBI on LHD. Top: Schematic view of beam accelerator. The steering grid provides a displacement δ_S to correct the beamlet trajectories. Bottom: The MSGG before installation in the new ion source. The long side of slits corresponds to *x*-direction.

Beam convergence

Computer simulations with semi-empirical beam parameters were used to design the new grids. Characteristics of beam convergence on the MSGG were also examined by measuring actual extracted beams. A calorimeter array is installed in the beam line 8.4 m from the grounded grid. Beam profiles in the *x*- and *y*-directions were measured by the array.

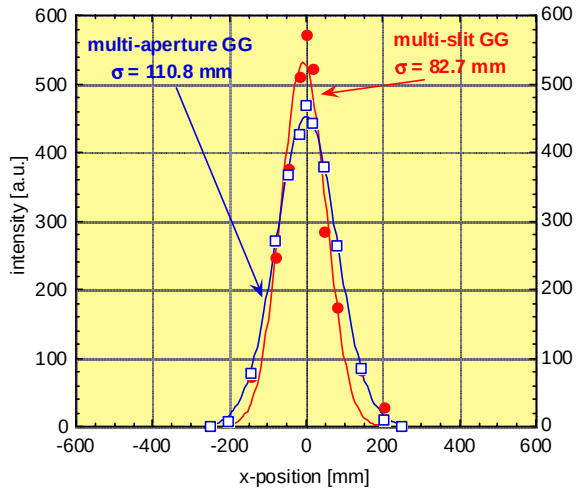

Fig. 3(a). Typical beam profiles in the *x*-direction obtained from the MAGG (blue open squares) and the MSGG (red solid circles).

.

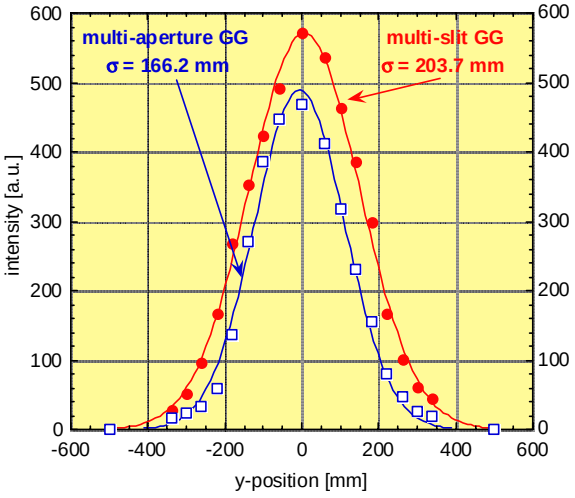

Fig. 3(b). Beam profiles in *y*-direction obtained from the MAGG (blue open squares) and the MSGG (red solid circles).

As shown in Fig. 3(a), the horizontal (*x*-direction) beam profile for the MSGG is narrower than the profile with the MAGG. It is experimentally verified that multi beamlets converge well in along the direction of a slit. In contrast, as shown in Fig. 3(b), the e-folding width in the *y*-direction, 204 mm, was wider the width than on the MAGG, 166 mm

Changes of the beam widths in the *x*- and *y*-directions are plotted as functions of the ratio of acceleration voltage V_{ac} to extraction voltage V_{ex}, R_V in Fig. 4.

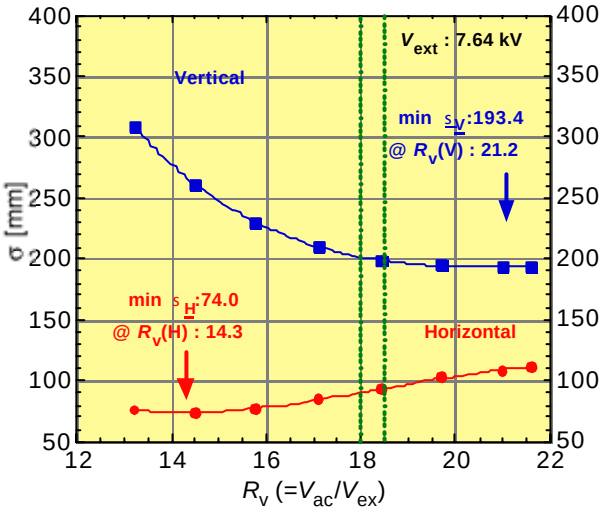

Fig. 4. Dependence of the *x* and *y* beam widths on the voltage ratio R_v, the ratio of acceleration voltage V_{ac} to extraction voltage V_{ex}. The beam is usually operated at ratios of 18–18.5 (area surrounded by green lines).

There remain two problems in beam convergence with the MSGG. The first is a mismatch of the minimum points of the *x* and *y* beam widths. The second is that the minimum width in *y*-direction is too large; it should be less than 165 mm. The displacement value of the steering aperture, which was calculated in the beam simulation, showed an error in the beam steering in the *y*-direction. Consequently, beam trajectories, after passing the MSGG, expand in *y*, even though the H^- beam passes through the MSGG. Because of its wider profile, the H^- beam touches the molybdenum protection armor on the injection port. Though the total injection power increases with an MSGG, the port through ratio is cut more than 10% lower than it is with the MAGG. The problem will be resolved by reoptimizing the steering grid before the next LHD experimental campaign.

Beam heat onto the grounded grid

When the focal condition and the steering condition are both satisfied, most of the H^- beam passes through each grid. However, some part of the extracted beam, such as the defocused H^- beam, the neutralized H^0 beam, and the electron beam, collides with the surface of the grids. Those beams sputter neutral particles and positive ions from grid surfaces. The beams also heat the grid, leading to desorption of gases from the grids. Sputtered ions and desorbed gases are expected to cause breakdowns between the grids, and extreme heat deposition can melt the grids. The heat load onto the grounded grid (GG) is much larger than the load on the EG, because the acceleration voltage is about 20 times as large as the extraction voltage. Reduction of the heat load on the grounded grid increases the product of the injection power and the beam pulse duration.

The grid contains water-cooling channels, and the heat load onto the grid is evaluated by measuring the water flow rate and the difference in water temperature between outlet and inlet water ports. Time variations of the temperature differences at the extraction grid $\Delta T_{EG}(t)$ and the grounded grid $\Delta T_{GG}(t)$ are shown in Fig. 5. The figure shows that the heat load on the EG (blue area) is much less than that on the GG (red area). The peak position of $\Delta T_{EG}(t)$ is delayed about 3 s from the peak position of $\Delta T_{GG}(t)$. The time delay is related to the distances between the heated position and the water channels inside the extraction and grounded grids. Here the peak of temperature difference at the grounded grid is defined as $\Delta T_{GG}(t)$ (max), and the heat load on the GG is indicated as Q_{GG}.

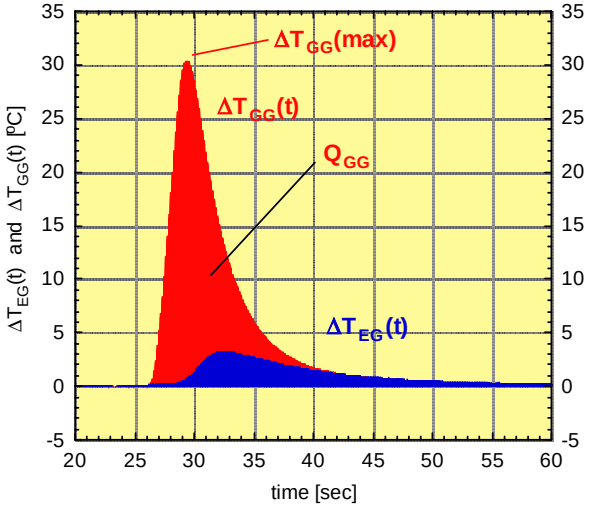

Fig. 5. Difference of outlet and inlet water temperatures at the extraction grid (blue area) and grounded grid (red area). The peak of temperature difference, $\Delta T_{GG}(t)$, is defined as ΔT_{GG}(max) and the area under the $\Delta T_{GG}(t)$ curve is the heat load on the grounded grid Q_{GG}.

In Fig. 6, peak temperatures of the MAGG and MSGG are plotted as functions of injection heat. The peaks are obtained by averaging through all of the grounded grids. The peak temperatures go up linearly with increasing injection heat. The temperature limits for the MAGG and MSGG are indicated as dotted lines, and the values are about 35°C and 40°C. These temperature limits represent the empirical values to melt the grids. The limits on injection heat are the points at which the peak temperature lines cross the temperature limits, ~8.5 MJ for the MAGG and ~16 MJ for the MSGG. The limit on the injection heat for the MSGG is twice as high as that for the previous MAGG

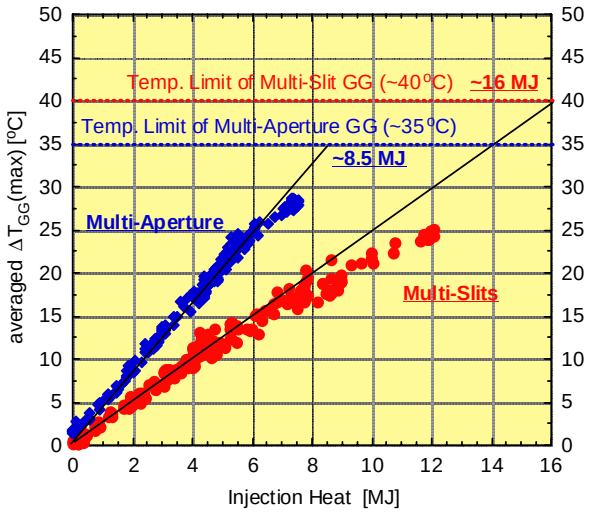

Fig. 6. Temperature rise of the grounded grids as functions of injection heat. The blue and red points are for the MAGG and MSGG grids, respectively.

The ratio of heat load on the grounded grids to the acceleration heat is plotted in Fig. 7. Here the acceleration heat is defined as the product of acceleration current, beam energy, and pulse duration. The figure shows that the heat on the grounded grids is a linear function of the acceleration heat, and 7.3% of acceleration heat is deposited to the MSGG.

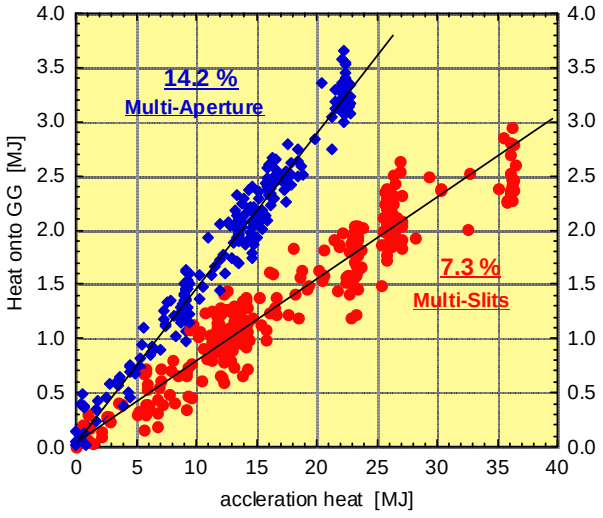

Fig. 7. Heat load on the MAGG (blue points) and MSGG (red points). The loads are proportional to acceleration heat.

Beam performance

Progress in the conditioning of beam energy is shown in Fig. 8. For the previous ion source, the maximum beam energy was 167 keV and it took about 1.2 months (about 5000 shots) to reach this value. With the new grids, we could reach the maximum energy of 180 keV in just 4 days (about 800 shots). The time is dominated by the cesium dose into the arc chamber.

This speedy conditioning changes the experimental use of NBI. Daily conditioning before an injection experiment is very short, and it is no longer necessary to do conditioning after each NBI experiment.

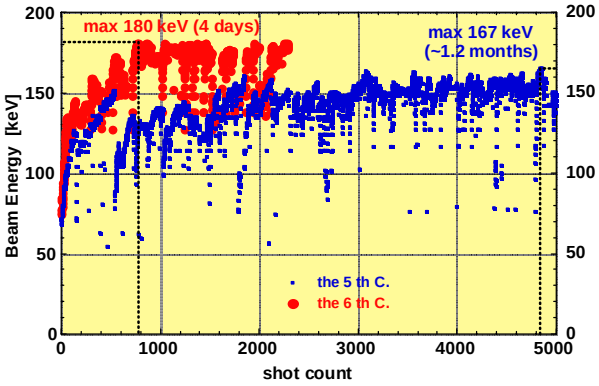

Fig. 8. Conditioning is much shorter using the MSGG (red) than it is with MAGG (blue).

Improvement in the NBI power as a function of beam energy, $E_{b,}$ is shown in Fig. 9. The colors indicate different periods in the experimental campaign. Injection power is proportional to $E_b^{5/2}$. The beam energy and injection power have also increased drastically. There was a barrier at an energy of 170 keV with the MAGG. The MSGG can jump the barrier and attain many times the 180-keV energy, with a pulse duration of 2 s even during beam injection. The maximum NBI power is 4.3 MW, and a power of 4.5 MW is obtained during conditioning by applying the port-through ratio.

Conclusion

In order to increase NBI power and make progress towards our mission, MSGGs have been used on a negative hydrogen ion source. The transparency of an MSGG is as about twice as large as that of an MAGG. Due to the large transparency, the heat load with an MSGG is reduced and it was able to inject a beam with over 4 MW of power. Our goal is partially achieved; namely, a beam energy of 180 keV has been reached. Conditioning time is also drastically reduced with the MSGG.

Due to the beam deposition optimization in LHD, the design values of beam energy and current for LHD negative NBI systems are different from those for large toka-

maks (relatively lower energy and higher current for LHD). However, since heat deposition on the grids is a general problem leading to the breakdown of any kind of high-power NBI system, the MSGG design could also be a breakthrough in developing negative ion NBI systems for tokamaks.

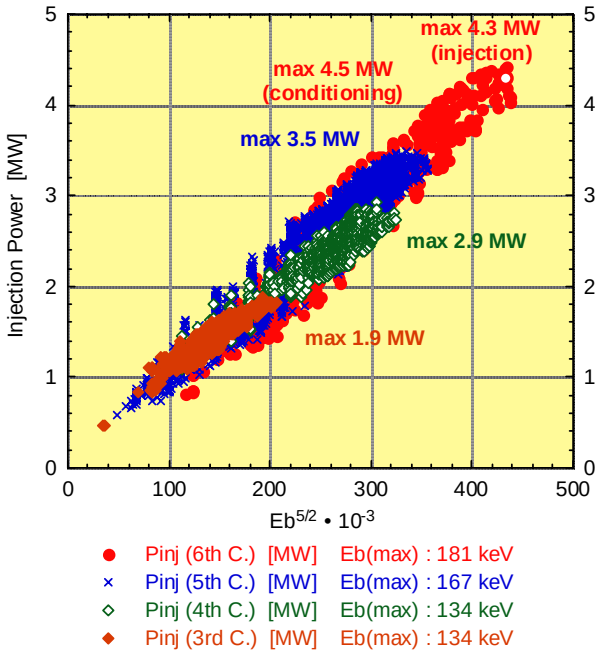

Fig. 9. Improvement of beam energy and injection power over the LHD experimental cycles.

Acknowledgment

The author thanks all the members of the LHD NBI group. The author also sends a special thanks to the people at Toshiba Co. Ltd. who helped us to construct the new negative ion source.

K.Tsumori
National Institute for Fusion Science
Toki, 509-5292, Japan
E-mail: Tsumori@nifs.ac.jp

References

[1] O. Kaneko, Y. Takeiri, K.Tsumori, Y. Oka, M. Osakabe, et al., Nucl. Fusion **42** (2002) 441–447.

[2] K. Tsumori, T. Takanashi, S. Asano, M. Osakabe, et al., *Proc. 8th Int. Symp. Production and Neutralization of Negative Ions and Beams*, France, pp. 93–104.

Meeting announcements

14th International Stellarator Workshop
September 22–26, 2003

Innovative Concepts and Theory of Stellarators
September 29–October 1, 2003

Greifswald, Germany

We are pleased to announce the 14th International Stellarator Workshop and the IAEA Technical Meeting on Innovative Concepts and Theory of Stellarators to be held in Greifswald, Germany. The workshops are being organized by the Max-Planck-Institut für Plasmaphysik in the framework of the International Energy Agency Implementing Agreement on the Stellarator Concept and in cooperation with the International Atomic Energy Agency (IAEA).

The Stellarator Workshop covers all areas of fusion research on helical systems and related concepts.

The aim of the IAEA Technical Meeting will be to cover technical issues in the theory of stellarators, so that this satellite meeting will be dominated by the discussion of progress of computational efforts.

Overviews in this area of research should be placed in the main workshop.

The workshop Web page

http://www.ipp.mpg.de/stellarator-workshop/

will provide information about deadlines, scientific program, schedule, and other organizational aspects.

In order to determine approximate attendance, we request that prospective attendees send the contact details requested on the Web page by e-mail or by fax and indicate their interest in either or both workshops.

E-mail: stellarator-workshop@ipp.mpg.de
Postal mail: Max-Planck-Institut für Plasmaphysik
Wendelsteinstrasse 1
D-17491 Greifswald
Germany
Phone: +49 3834 88 2005
Fax: +49 3834 88 2009

Extended abstracts

A new quasi-stationary, very high density plasma regime on the W7-AS stellarator

Plasma Phys. Controlled Fusion **44** (2002) 193–205 (invited papers of the 29th EPS Conference, 2002), on line at stacks.iop.org/PPCF/44/B193

Stellarators have the intrinsic property of steady state operation. However, on present-day stellarators the pulse length is usually limited not only due to technical reasons, but also by physical problems. Lack of density control and a subsequent radiation collapse terminate the discharges quite often at high densities. To improve the control of the plasma-wall interaction, the island divertor concept was developed for optimized stellarators. To test this divertor concept on W7-AS, all limiters were removed and replaced by ten divertor modules. In subsequent divertor experiments a promising new plasma operational regime has been discovered which is termed “high density H-mode” (HDH-mode). During the transition into that regime a clear reduction of ELM-like events and turbulent fluctuations is observed. The HDH-mode combines good energy confinement with very low impurity confinement resulting in low core radiation, but high edge-localized radiation. Consequently, stationary discharges at densities of typically 2×10^{20} m^{-3} can be performed within the accessible pulse length of about 1 s. At densities above 3×10^{20} m^{-3} a controlled transition from attached to partially detached plasmas is observed. The still edge-localized radiation reaches 90% of the heating power so that the power load onto the divertor target plates is further reduced. At a lower toroidal field of 0.9 T average beta values could be raised from earlier 2% to more than 3% in magnetic field configurations with rather smooth flux surfaces at the plasma boundary. The recently obtained results render excellent prospects for W7-X, the larger superconducting successor experiment of W7-AS.

R. Jaenicke, S. Baeumel, J. Baldzuhn, R. Brakel, R. Burhenn, H. Ehmler, M. Endler, V. Erckmann, Y. Feng, F. Gadelmeier, J. Geiger, L. Giannone, P. Grigull, H. J. Hartfuss, D. Hartmann, D. Hildebrandt, M. Hirsch, E. Holzhauer, M. Kick, J. Kisslinger, T. Klinger, S. Klose, J. Knauer, R. Koenig, G. Kuehner, H. Laqua, H. Maassberg, K. McCormick, R. Narayanan, H. Niedermeyer, E. Pasch, N. Ruhs, N. Rust, J. Saffert, F. Sardei, F. Schneider, M. Schubert, E. Speth, F. Wagner, A. Weller, U. Wenzel, A. Werner, E. Wuersching

Max-Planck Institut für Plasmaphysik
EURATOM-Association
D-85748 Garching, Germany

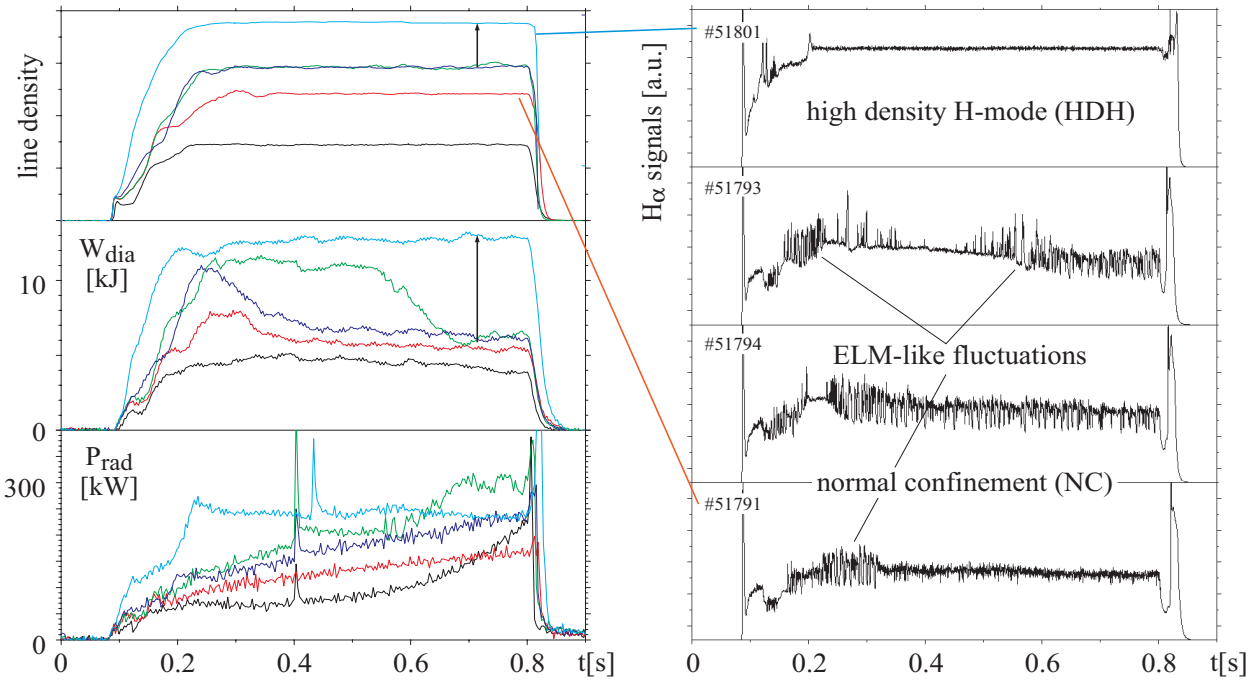

Fig. 1. Density scan on W7-AS after the installation of divertor modules. At left: line density (corresponding to line-averaged densities of 0.7 to 2×10^{20} m^{-3}, diamagnetic energy content W_{dia}, and total radiation P_{rad}. At right the disappearance of ELM-like events during the transition from normal confinement to the HDH-mode is demonstrated. Common discharge parameters are: B_0 = 2.5 T, $\iota(a) \approx 5/9$ (divertor magnetic field configuration) and 0.7 MW NB heating power.

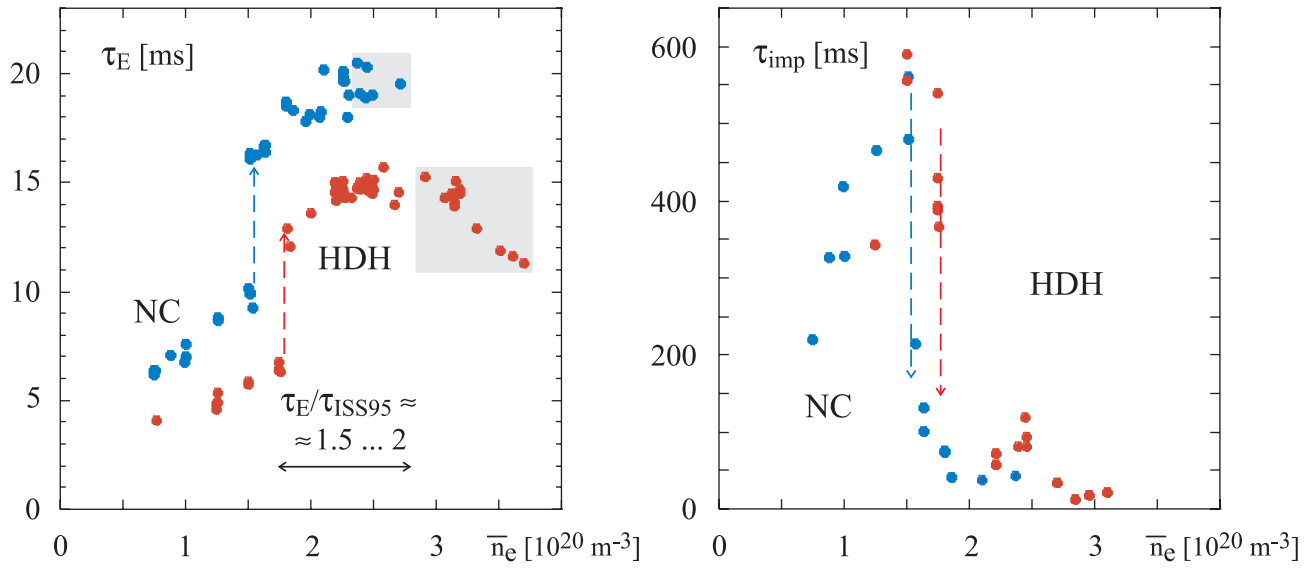

Fig. 2. Change of global transport properties during the transition from normal confinement (NC) to the HDH-mode. Shown are the energy confinement time τ_E and impurity confinement time τ_{imp} (exponential decay time of laser-ablated aluminum) versus line-averaged density for divertor discharges with about 0.7 and 1.3 MW of neutral beam heating power (2 and 4 neutral beam sources, respectively). Broken vertical lines point out that the transition takes place within a narrow density range. Shaded ranges indicate partial detached states.

Investigation of the beta-limit in the W7-AS Stellarator

A significant increase of the volume-averaged beta from $\beta \sim 2\%$ up to $\beta > 3\%$ was achieved in W7-AS after modifications of the neutral beam injection (NBI) system and the installation of divertor structures. In particular, the favorable properties of high-iota configurations could be exploited by using the divertor control coils for eliminating edge islands. MHD-quiescent, quasi-stationary discharges at low radiation levels and with favorable confinement properties can be maintained.

The discharge properties at high beta are very similar to those in the High Density H-Mode regime first found in proper island divertor configurations. Experimental studies of equilibrium effects and of MHD mode activity have been performed with the X-ray tomography system for a variety of magnetic configurations. Experimental evidence of effects of the advanced configuration is obtained from comparison of the X-ray data with free boundary equilibrium calculations. In addition, results of computational MHD stability studies are presented, which show an increase of stability with increasing beta due to the pressure induced deepening of the magnetic well along with increasing magnetic shear, in qualitative agreement with experimental data. Under typical conditions the maximum achieved beta is still limited by the available heating power and not by equilibrium or stability effects. If the plasma is pushed close to the density limit or in the case of significant toroidal current drive, MHD instabilities may cause a deterioration of the confinement. The reduced beta obtained in low-iota configurations is attributed to the equilibrium beta limit due to a critical Shafranov shift associated with enhanced transport.

A. Weller,[1] J. Geiger,[1] M. Zarnstorff,[2] E. Sallander,[1] S.Klose,[1] A. Werne,[1] J.Baldzuhn,[1] R. Brakel,[1] R. Burhenn,[1] H. Ehmler,[1] F. Gadelmeier,[1] L. Giannone,[1] D.Hartmann,[1] R. Jaenicke,[1] J.Knauer,[1] H.P.Laqua,[1] C.Nührenberg,[1] E. Pasch,[1] N.Rust,[1] E.Speth,[1] D.A.Spong,[3] F.Wagner,[1] U. Wenzel,[1] W7–AS Team[1], NBI-Group[1]

1. Max-Planck-Institut für Plasmaphysik, IPP-Euratom Association, D-85748 Garching, D-17489 Greifswald, D-10117 Berlin, Germany

2. Princeton Plasma Physics Laboratory, Princeton, NJ 08543, USA

3. Oak Ridge National Laboratory, Oak Ridge, TN 37831-8071, USA

E-mail: arthur.weller@ipp.mpg.de

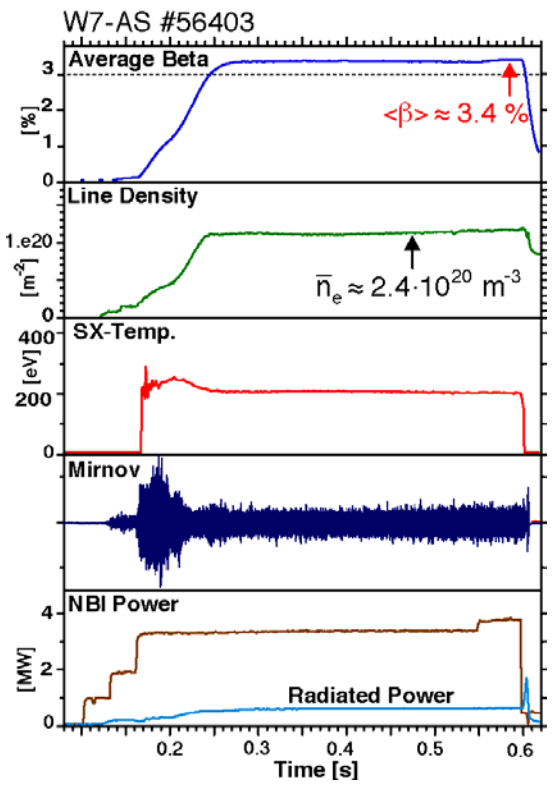

Fig. 1. Optimized quasi-stationary high-beta discharge at 0.9 T, ι_{ext} = 0.52, with $\langle\beta\rangle$ reaching 3.4%. The (low) radiation losses are peaked at the plasma edge.